Acoustic radiation of a fluid-saturated microperforated plate

Lucie Gallerand, Mathias Legrand, Thomas Dupont, Raymond Panneton, Philippe Leclaire

25-29 August 2024
inter.noise
NANTES FRANCE

Acoustic radiation of a fluid-saturated microperforated plate

Lucie Gallerand [1]
Department of Mechanical Engineering, École de technologie supérieure
Montréal, Canada

Mathias Legrand
Department of Mechanical Engineering, McGill University
Montréal, Canada

Thomas Dupont
Department of Mechanical Engineering, École de technologie supérieure
Montréal, Canada

Raymond Panneton
CRASH-UdeS, Department of Mechanical Engineering, Université de Sheerbroke
Sheerbroke, Canada

Philippe Leclaire
DRIVE EA1859, Université de Bourgogne Franche-Comté, ISAT
Nevers, France

ABSTRACT

It is known that fluid-saturated microperforated plates (MPP) dissipate energy and are substantially damped through thermoviscous dissipation taking place in the thermoviscous skin on the solid wall of the perforations. The aim of this work is to explore the acoustic radiation of a microperforated periodic cell to investigate the intercellular coupling and the complexity of near-field radiation, and to derive a criterion related to the near-field far-field transition. A numerical modeling using the finite element method is developed to solve the elastic and thermo-visco-acoustic (TVA) multiphysics problem. The TVA calculates explicitly the thermoviscous losses on the acoustic wave in the periodic cell studied. Numerical results show that the distance of the near-far field transition is significant at low frequencies, passing through a minimum for a frequency depending on perforation parameters (diameter and ratio) before increasing again as a frequency function. The radiated acoustic power and radiation efficiency are compared with those derived from the theoretical MPP vibration model. It is found that the microperforations and resulting added damping, around a characteristic frequency, reduce the acoustic radiation efficiency of the MPP compared to the corresponding non-perforated plate.

1. INTRODUCTION

Microperforated plates (MPP) dissipates energy through the coupling of reactive and resistive effects of a viscothermal nature [1]. These mechanisms are widely used to improve acoustic absorption,

[1]lucie.gallerand.1@ens.etsmtl.ca

but also have an influence on the dynamic behavior of the MPP. However, few research studies have focused on the influence of viscous dissipation on MPP dynamics. Studies have focused mainly on i) the influence of vibration on the acoustic response of the plate [2–4], ii) acoustic radiation [2–4] and iii) acoustic transmission [4, 5].

A previous work by the authors [6] proposed to use MPP to reduce the contribution of low-frequency modes of vibration in the response. Due to the thermoviscous interactions occurring in the thermoviscous skin on the solid wall of the perforations, these systems dissipate vibratory energy efficiently. The dissipation mechanism reaches a maximum at a given *characteristic frequency*, and increases in significance the more this frequency is in the low-frequency range. For MPP whose perforation diameter is of the order of the boundary layer thickness, the motion of the solid part of the MPP will drive the fluid into the microperforations. During motion of the plate in a fluid environment, it radiates acoustic waves, which are the source of structure-borne noise. In the case of an MPP, two elements are radiated: i) the fluid in the perforations, ii) the solid part of the MPP. The added damping exhibited by MPP can have an influence on the acoustic radiation of the structure.

The vibration of fluid-saturated porous plate was already explored [7] by using the classical approach of radiated plate [8]. However, it is now established that MPP can be identified with equivalent porous plates [9].

This contribution propose therefore to investigate the influence of the added damping on the acoustic radiation of an MPP saturated by lightweight fluid. It is organized as follows. First in Section 2 the equations of motion for a microperforated plate moved by a light fluid are established. Section 3 details the implemented finite element model and Section 4 discusses the results.

2. THEORETICAL BACKGROUND

2.1. Equations of motion of the fluid-saturated microperforated plate

The investigated structure is a cantilever rectangular microperforated plate (MPP) of dimension $L_x \times L_y \times h$ oriented in the (x, y)-plane immersed into a fluid domain. The MPP is placed in a rectangular opening in a rigid, immobile wall separating two fluid media. The plate can be excited mechanically by a driving external force $f_{\text{ext}}(\mathbf{x}, t)$, acoustically by a pressure difference $\Delta P(\mathbf{x}, t)$ between the plane $z = -h/2$ and $z = +h/2$, or acoustically and mechanically through a combination of the two external excitations. The point $\mathbf{x} \equiv (x, y)$ defines the transverse coordinates. Using an alternative form of Biot's theory, the model developed in the framework of porous plates in [10] is adapted to the considered MPP. An *ad hoc* homogenization procedure is performed, leading to two coupled partial differential equations (PDEs) that govern the dynamics of a structural plate and a virtual fluid plate [6]:

$$h(\rho\, \ddot{w}_{\text{s}}(\mathbf{x}, t) + \rho_{\text{f}} \ddot{w}(\mathbf{x}, t)) + D(\phi)\nabla^4 w_{\text{s}}(\mathbf{x}, t) = f_{\text{ext}}(\mathbf{x}, t), \tag{1a}$$

$$\rho_{\text{f}} h \ddot{w}_{\text{s}}(\mathbf{x}, t) + \frac{h\rho_{\text{f}}\alpha_\infty}{\phi} \ddot{w}(\mathbf{x}, t) + h\sigma \dot{w}(\mathbf{x}, t) + h\alpha M_{\text{f}} \nabla^2 w_{\text{s}}(\mathbf{x}, t) = \Delta P(\mathbf{x}, t), \tag{1b}$$

where $w_{\text{s}}(\mathbf{x}, t)$ is the solid motion displacement and $w(\mathbf{x}, t)$ corresponds to the relative fluid-solid motion displacement. Obtained by identifying the MPP with a porous plate [9], they account for the vibratory behavior of the MPP. The pressure difference ΔP corresponds to the boundary conditions applied to the fluid at $z = -h/2$ and $z = h/2$. For a purely mechanical excitation, the term $\Delta P(\mathbf{x}, t)$ is set to zero. For a purely acoustic excitation, at the surface of the plate, the total pressure exciting the plate is the blocked pressure. Thus, the external loading in Equation (1a) corresponds to the blocked pressure $2P$ with P the incident pressure [11], while that applied to Equation (1b) corresponds to ϕP [10]. In the remainder, only a purely mechanical excitation is considered.

In Equation (1a), the fluid-solid mixture density is described by $\rho = (1 - \phi)\rho_{\text{s}} + \phi\rho_{\text{f}}$ where ρ_{s} and ρ_{f} are respectively the solid and the fluid density with ϕ, the perforation ratio. In order to consider the influence of the microperforations in the MPP stiffness, the bending stiffness

coefficient reads

$$D(\phi) = \frac{EC(\phi)h^3}{12(1-\nu^2)} \quad \text{with} \quad C(\phi) = \frac{(1-\phi)^2}{1+(2-3\nu)\phi} \tag{2}$$

where E and ν are respectively Young's modulus and Poisson's ratio of the non-perforated plate. The parameters α and M_f are the elastic coefficients defined by Biot [12]. Equation (1a) represents the elastic response of the homogeneous solid plate while Equation (1b) describes the relative fluid-solid motion. Elastic interactions are quantified by the α-dependent term. Inertial interactions are described by the acceleration terms. In this model, all Johnson-Champoux-Allard (JCA) parameters defined for a porous medium can be translated to an MPP as being functions of ϕ and d. Accordingly, resistivity and tortuosity are defined by

$$\sigma_0(\phi, d) = \frac{32\mu_\mathrm{f}}{\phi d^2} \quad \text{and} \quad \alpha_\infty(\phi, d) = 1 + \frac{2\epsilon(\phi, d)}{h} \tag{3}$$

where μ_f is the fluid dynamic viscosity and $\epsilon(\phi, d) = 0.24\sqrt{\pi d^2}(1 - 1.14\sqrt{\phi})$ [9] is an end correction factor used to consider the fluid radiation inside the perforations and the distortion of the fluid flow at the perforation orifices. Details about the analytical resolution are given in [6]. For an MPP, the added damping is maximal at the *characteristic frequency* [6]

$$f_\mathrm{c}(d) = \frac{32\mu_\mathrm{f}}{2\pi\alpha_\infty\rho_\mathrm{f}d^2} \tag{4}$$

where d can be adjusted to induce maximum added damping at the resonance frequency by forcing $f_\mathrm{c}(d)$ to coincide with a resonance frequency of the MPP.

2.2. Radiation impedance

The acoustic radiation of a vibrating MPP immersed in a fluid domain is considered in this section. In addition to the fluid in the perforations, it is then necessary to consider the external fluid loading on the structure and the resulting fluid-structure interaction. Since the MPP appears as a continuous medium at the wavelength scale, the results of classical plate theory can be applied. Fluid loading is introduced into the equations of motion by the addition of a coupling term, dependent on $w_\mathrm{s}(\mathbf{x}, t)$. This acoustic source involves the acoustic radiation impedance and is expressed as

$$q_i(\mathbf{x}, t) = -j\omega \sum_{k=1}^{\infty} Z_{ik}(\omega)(1-\phi)\, w_k^\mathrm{s}(t)\Psi_k(\mathbf{x}), \tag{5}$$

where the radiation matrix impedance given by

$$Z_{ik}(\omega) = j\omega\rho_\mathrm{f}\int_S\int_{S_1} \Psi_i(\mathbf{x})G(\mathbf{x},\mathbf{x}_1)\Psi_k(\mathbf{x}_1)\mathrm{d}S_1\mathrm{d}S \quad \text{with} \quad k = (p, q), \tag{6}$$

is associated with the contribution of the surface elements S_1 and S. Equation (6) involves the position vector of a transmitting element $\mathbf{x}$ and a receiving element $\mathbf{x}_1$. In Equation (6), the Green function is defined for a half-space as

$$G(\mathbf{x},\mathbf{x}_1) = \frac{\exp(-j\omega\,\|\mathbf{x}-\mathbf{x}_1\|)}{2\pi c_0\,\|\mathbf{x}-\mathbf{x}_1\|}. \tag{7}$$

The operator $\|\cdot\|$ refers to the norm between $\mathbf{x}$ and $\mathbf{x}_1$ and c_0 is the fluid celerity. When the distance $\|\mathbf{x}-\mathbf{x}_1\|$ tends towards zero, Green's function becomes singular. To deal with this singularity and ensure numerical convergence of the integral, a quadruple Riemann sum is performed to obtain an approximation of Equation (6).

2.3. Vibroacoustic indicators

The three main vibroacoustic indicators are calculated in this work: (1) the radiated sound power that corresponds to the sound energy radiated by the baffled microperforated plate; (2) the mean square velocity that leads to the global dynamic behaviour of the MPP; (3) the radiation efficiency the expresses the part of the vibration energy that is transformed into sound. Radiated sound power is defined as the integration of sound intensity over the surface of the plate over a period of time, that is

$$W(\omega) = \frac{\omega}{2\pi} \int_0^{\frac{2\pi}{\omega}} \int_S P(\mathbf{x}, t)\, \dot{w}_{\text{tot}}(\mathbf{x}, t)\, \mathrm{d}S\mathrm{d}t \tag{8}$$

where $w_{\text{tot}}(x, t) = w_{\text{s}}(\mathbf{x}, t) + w(\mathbf{x}, t)$ is displacement field in the vicinity of the plate surface. The function $P(\mathbf{x}, t)$ is the surface acoustic pressure given by

$$P(\mathbf{x}, t) = -\rho_{\text{f}}\omega^2 \int_{S_1} w_{\text{tot}}(\mathbf{x}_1, t) G(\mathbf{x}, \mathbf{x}_1) \mathrm{d}S_1. \tag{9}$$

The mean square velocity is the space-time average of the squared velocity of the plate

$$V^2(\omega) = \frac{\omega}{2\pi L_x L_y} \int_0^{\frac{2\pi}{\omega}} \int_S |\dot{w}_{\text{tot}}(\mathbf{x}, t)|^2 \mathrm{d}S\mathrm{d}t. \tag{10}$$

From radiated sound power and the mean square velocity derives the acoustic radiation efficiency

$$s(\omega) = \frac{W(\omega)}{\rho_{\text{f}} c_0 V^2(\omega) L_x L_y}. \tag{11}$$

3. FINITE ELEMENT MODELING

In order to validate the model proposed in Section 2, an MPP embedded in a fluid medium is considered as schematized in Figure 1. The losses occurring in the thermal and viscous boundary layers near the walls are considered by solving the equations of the thermoviscous problem (the linearized Navier-Stokes equations). These equations are implemented in the COMSOL Multiphysics software package in the Thermovisous Acoustics module (TVA) [13].

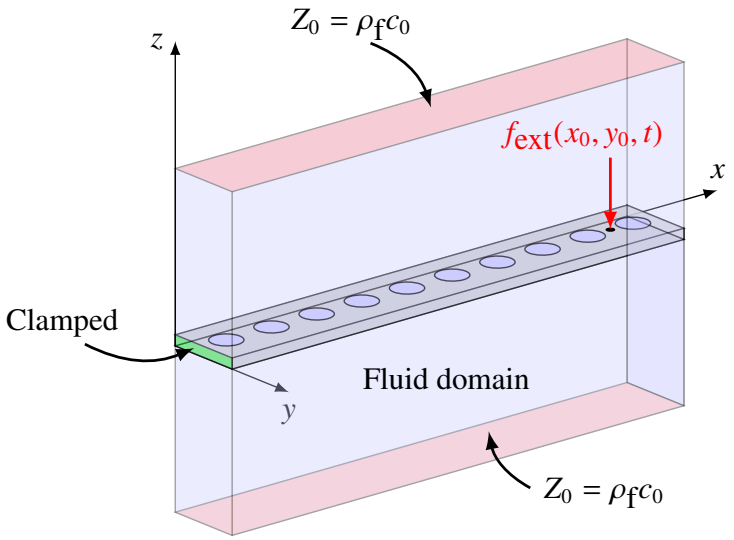

Figure 1: MPP of dimension 131 mm × 30.7 mm × 1 mm clamped at $x = 0$ and mechanically excited at abscissa x_0. The diameter of the perforations $d = 1$ mm is chosen to maximize the damping added to the first MPP mode, and the perforation ratio is $\phi = 10\,\%$. The far field is modeled by applying an impedance Z_0 on both sides of the fluid domain. The fluid in the perforations is modeled using the TVA approach to account for visco-thermal losses.

The mechanical parameters of the MPP are listed in Table 1. The finite-size MPP is enclosed in a baffle that separates two external air environments, enabling the acoustic load on both surfaces (at $z = -h/2$ and $z = h/2$) of the MPP to be considered. A pointwise forcing $f_{\text{ext}}(x, y, t)$ of amplitude $F_{\text{ext}} = 1\,\text{N}$ is applied at the point $(x_0, y_0) = (115.65\,\text{mm}, 30.7\,\text{mm})$. In Figure 1, the far field is modelled

Microperforated plate		**Fluid and solid mechanical parameters**	
L_x (mm)	131	ρ_s (kg m^{-3})	7850
L_y (mm)	30.7	ρ_f (kg m^{-3})	1.213
h (mm)	1.0	E (GPa)	203
ϕ (%)	10	ν	0.3
d (mm)	1	η_s	10^{-4}

Table 1: Numerical values implemented in the finite element modeling.

by applying the impedance $Z_0 = \rho_0 c_0$ at $z = \pm 700\,\text{mm}$. As the analytical model is homogenized, the radiated sound pressure is calculated by EF far from the perforations at $z = 700\,\text{mm}$, to compare the numerical and theoretical predictions. In fact, local radiation close to the perforations develops into a cylindrical wave at medium distance and then becomes flat in the far field.

The TVA interface is governed by the equation of continuity, the equation of conservation of momentum and the equation of conservation of energy. These equations are solved, between 10 Hz and 90 Hz with a frequency step of 5 Hz, in conjunction with the bending equations governing the dynamics of the solid part of the MPP. Around the fist MPP resonance $f_1 \approx 48\,\text{Hz}$, a frequency refinement with a step size of 0.5 Hz is performed. Analytical and numerical results are presented in Section 4.

4. RESULTS AND DISCUSSIONS

In Figure 2, the analytical acoustic radiation efficiency obtained from Equation (11) is presented. The MPP is compared to the reference non-perforated plate.

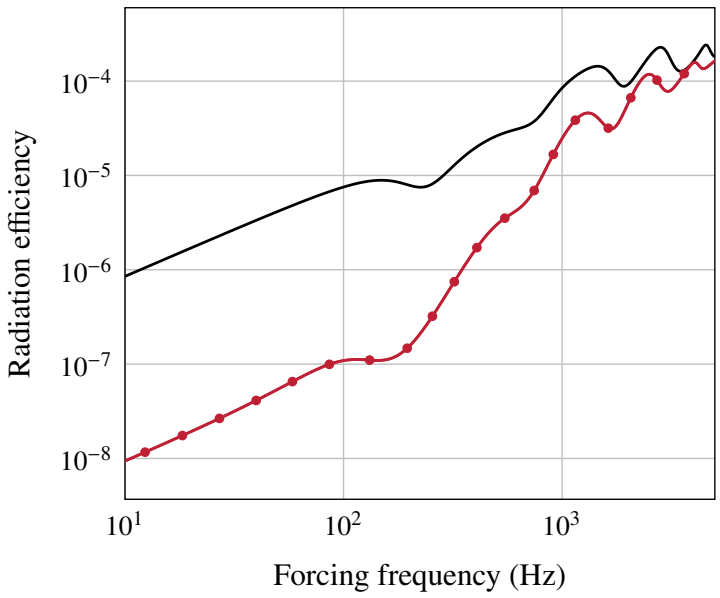

Figure 2: Radiation efficiency as a function of the forcing frequency obtained via Equation (11): (—•—) MPP described in Table 1, (——) reference non-perforated plate.

The perforation diameters are chosen to induce maximum added damping around the

first vibration mode of the MPP. Figure 2 shows that the acoustic radiation efficiency decreases substantially between microperforated and nonperforated plates. The presence of perforations on the structure reduces its density, rigidity and thus its radiating surface. Moreover, in Figure 2, the reduction in acoustic radiation efficiency is greater in the low-frequency range for the MPP than for the reference plate without perforation. This is because the damping added by the perforations, which is a low frequency effect acting around the characteristic frequency and reduces the amplitude of displacement of the structure. The result is a reduction in acoustic radiation. The result is a reduction in acoustic radiation in the low-frequency range. The added damping effect has no influence in the high-frequency range, thus the reduction in radiation efficiency is due exclusively to the reduction in radiating surface.

The finite element modeling presented in Section 3 is used to validate the analytical model. Only the first MPP resonance is considered here in order to observe the influence of dissipative effects, which are maximal around f_1. The radiated sound power is obtained using both methods (analytical from Equation (8) and finite element) and is presented in Figure 3.

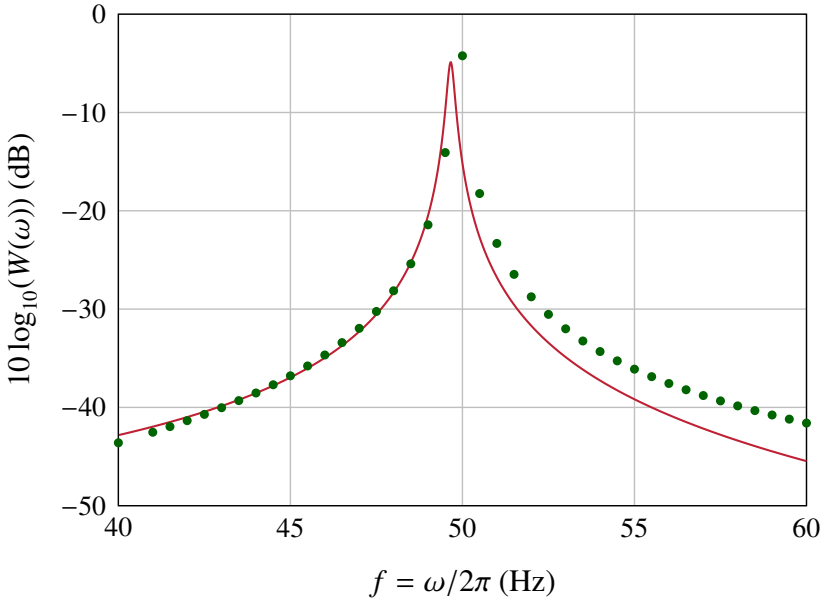

Figure 3: Radiated acoustic power obtained as : (•) finite element method; (—) analytical approach via Equation (8). The parameters of the cantilevered MPP considered are given in Table 1.

Comparisons between analytical results and those provided by the finite element method validate the analytical model.

5. CONCLUSION

This paper suggested to apply classical plate acoustic radiation theory in order to explore the MPP acoustic radiation. Homogeneous fluid and solid vibration fields were calculated from the analytical model proposed in [6]. It was shown analytically that under mechanical and acoustic excitation, microperforations significantly reduce the structural acoustic radiation efficiency around the characteristic frequency. In fact, the reduction in acoustic radiation is due to i) the reduction in radiating surface induced by the microperforations and ii) the reduction in vibration amplitude due to the added damping resulting from visco-thermal dissipation in the perforations around the characteristic frequency. Numerical modeling using the finite element method was also implemented to solve the multiphysics elastic and thermo-visco-acoustic (TVA) problem, validating the proposed model.

REFERENCES

1. D.-Y. Maa. Potential of microperforated panel absorber. *Journal of the Acoustical Society of America*, 104:2861, 1997. [DOI].
2. Y.Y. Lee, E.W.M. Lee, and C.F. Ng. Sound absorption of a finite flexible micro-perforated panel backed by an air cavity. *Journal of Sound and Vibration*, 287:227–243, 2005. [DOI].
3. D. Takahashi and M. Tanaka. Flexural vibration of perforated plates and porous elastic materials under acoustic loading. *Journal of the Acoustical Society of America*, 112(4):1456–1464, 2002. [DOI],[OA].
4. T. Bravo, C. Maury, and C. Pinhède. Vibroacoustic properties of thin micro-perforated panel absorbers. *Journal of the Acoustical Society of America*, 132:789–798, 2012. [DOI].
5. T. Dupont, G. Pavic, and B. Laulagnet. Acoustic properties of lightweight micro-perforated plate systems. *Acta Acustica united with Acustica*, 89(2):201–212, 2003. [OA].
6. L. Gallerand, M. Legrand, T. Dupont, and P. Leclaire. Vibration and damping analysis of a thin finite-size microperforated plate. *Journal of Sound and Vibration*, 541:117295, 2022. [DOI], [OA].
7. H. Aygun, K. Attenborough, and A. Cummings. Predicted effects of fluid loading on the vibration of elastic porous plates. *Acta Acustica united with Acustica*, 93:6, 2007. [OA].
8. O. Foin, J. Nicolas, and N. Atalla. An efficient tool for predicting the structural acoustic and vibration response of sandwich plates in light or heavy fluid. *Applied Acoustics*, 57(3):213–242, 1999. [DOI].
9. N. Atalla and F. Sgard. Modeling of perforated plates and screens using rigid frame porous models. *Journal of Sound and Vibration*, 303:195–208, 2007. [DOI], [OA].
10. P. Leclaire, K.V. Horoshenkov, and A. Cummings. Transverse vibration of a thin rectangular porous plate saturated by a fluid. *Journal of Sound and Vibration*, 247(1):1–18, 2001. [DOI], [OA].
11. R. Panneton and N. Atalla. Numerical prediction of sound transmission through finite multilayer systems with poroelastic materials. *The Journal of the Acoustical Society of America*, 100(1):346–354, 1996. [DOI].
12. M.A. Biot and D.G. Willis. The elastic coefficients of the theory of consolidation. *Journal of Applied Mechanics*, pages 594–604, 1957. [DOI].
13. T. C. Kone, M. Lopez, S. Ghinet, T. Dupont, and R. Panneton. Thermoviscous-acoustic metamaterials to damp acoustic modes in complex shape geometries at low frequencies. *The Journal of the Acoustical Society of America*, 150(3):2272–2281, 2021. [DOI].